Coregistration of Interferometric SAR Images Using Spectral Diversity

Rolf Scheiber and Alberto Moreira, *Senior Member, IEEE*

***Abstract*—This article presents a technique for the determination of the relative misregistration between two interferometric SAR images. The proposed technique is based on the spectral properties of the complex SAR signal. Unlike conventional coregistration methods, the proposed technique does not need any interpolation nor cross-correlation procedures and also no coherence or fringe optimization must be performed. Instead, the phase information of different spectral looks is evaluated giving misregistration information on a pixel by pixel basis. The proposed technique is at least as accurate as the conventional algorithms and its implementation is very simple. Airborne repeat-pass interferometric data and simulated ScanSAR data are used to illustrate the operation of the proposed technique.**

***Index Terms*—Image registration, interferometry, repeat-pass interferometry, Scan-SAR, synthetic aperture radar (SAR).**

I. Introduction

INTERFEROMETRIC SAR imaging has become a useful technique for the generation of digital elevation models (DEMs) and also for the mapping of displacement fields on the order of the radar wavelength [1]–[3]. Additional information is often extracted for classification purposes. The data acquisition is performed in single- or repeat-pass mode by airborne or spaceborne sensors. At least two spatially or temporally separated images are needed to form an interferometric pair. After the phase preserving processing and filtering of the two images, a very precise coregistration step is required before the interferogram is generated. The precise coregistration increases the coherence of the interferogram, improves the quality of the phase unwrapping procedure, and leads to a more accurate phase in the final interferogram. If the coregistration errors are in the order of the geometric resolution, the coherence of the interferogram is significantly reduced and the phase noise is considerably increased.

Conventional techniques for coregistration are based on the cross correlation of the detected amplitude images and on the optimization of the fringe contrast or of the coherence [4], [1], [5]. In the first case, cross-correlation operations must be performed, and when an optimization procedure is employed, interpolations are required for each of the iterative loops. This leads to a large amount of computation. The commonly reported coregistration accuracy in the literature is in the order of 0.05 image samples [1].

Manuscript received August 31, 1999; revised April 18, 2000 and May 15, 2000.

The authors are withare with the Institut für Hochfrequenztechnik und Radarsysteme, Deutsches Zentrum für Luft- und Raumfahrt e.V., D-82230 Oberpfaffenhofen, Germany (e-mail: rolf.scheiber@dlr.de).

Publisher Item Identifier S 0196-2892(00)08917-8.

Several SAR-related techniques have already been developed that exploit the spectral properties of received complex signals for different purposes. In [6], the proportionality of the carrier frequency to the measured interferometric phase is used to generate two slightly different phase maps, which can be used for the calculation of the absolute phase offset prior to generating digital elevation models. In [7], [8], two dedicated different frequency channels are used for both antennas to generate a difference interferogram that can easily be unwrapped, leading to a more reliable unwrapping of the single channel interferogram.

The proposed technique for estimation of the coregistration errors is also based on spectral properties and relies on the well known fact that the impulse response function (IRF) of a SAR system has a linear phase variation within its mainlobe that directly depends on the center frequency of the data. The technique works as follows [9], [10]. Two sets of interferograms are generated having different azimuth or range center frequencies dependent on whether the misregistration in azimuth or range is to be estimated. The difference phase between the two interferograms is directly used to calculate the coregistration errors. No amplitude cross correlations nor interpolations for fractional shifts are needed. Selection of the spectral look separation and careful design of the coregistration strategy avoids any phase unwrapping of the measured difference phase. A simplified implementation of this method has also been used in [11] to efficiently solve the azimuth coregistration and coherent look summation problem for an interferometric quick-look processor. One of the methods presented in [6] for the determination of the interferometric absolute phase offset essentially performs the same operations with range looks but does not point out explicitly the inherent coregistration aspect.

In this paper, we present the general formulation of this spectral diversity technique, especially for estimation of the coregistration parameters in range and/or azimuth directions. This technique is further modified to estimate the coregistration error for ScanSAR data. Section II of this paper presents the analytical formulation of the proposed coregistration method for the stripmap case and also investigations on its accuracy. New aspects are presented concerning the coregistration of SAR images showing that the required coregistration accuracy increases considerably for high squint angles. In Section III, we address the azimuth coregistration problem for ScanSAR interferometry, and it is shown how to apply the spectral diversity technique to solve for the spectral and spatial misalignment. Section IV is dedicated to experimental results obtained with E-SAR data in the repeat-pass interferometric mode [12]. The ScanSAR coregistration case is illustrated using an ERS

0196–2892/00$10.00 © 2000 IEEE

tandem pair as a starting point for the simulation of the ASAR instrument of the ENVISAT platform in ScanSAR mode [13].

II. Coregistration by Spectral Diversity

The focused complex SAR signal formulation is essential for the modeling of the proposed spectral diversity technique for interferometric image coregistration purposes. Therefore, the impulse response function (IRF) obtained by the matched filter approach [14] is reviewed in the first section. Then, we reconsider the coregistration accuracy for a squinted geometry including a variation of the Doppler centroid along the range direction of the image. The spectral diversity technique is modeled next and its coregistration accuracy is estimated.

Since the technique works on one-dimensional (1-D) signals and there is no difference whether it is applied to the range or azimuth coregistration case, the modeling is also kept 1-D and is valid for both cases.

A. Matched Filter Focusing

In SAR raw data processing, especially in the stripmap case, focusing in either the range or azimuth directions is usually obtained by a matched filtering approach as part of a more complex algorithm [15]–[17]. Without loss of generality, let us consider a 1-D raw data SAR signal in range or azimuth with quadratic phase modulation, usually denoted as a chirp

$$s_1(t) = a(t - t_0 - t_c) \cdot e^{j\Phi_1} \cdot e^{j\pi k(t-t_0)^2}, \quad t \in \left[t_0 + t_c - \frac{T_1}{2}, t_0 + t_c + \frac{T_1}{2} \right] \tag{1}$$

where $a(t)$ is a real valued weighting function, Φ_1 is a constant signal phase, and k is the modulation rate. The time variable t of the signal of time duration T_1 is centered at $t_0 + t_c$, where t_0 defines the zero frequency position of the chirp, and t_c corresponds to a frequency offset f_{c1}. In the case of matched filtering in the frequency domain, the data is transformed to the Fourier space. For large time-bandwidth product signals, the following formulation can be found when applying the principle of stationary phase [18]:

$$S_1(f) = a(f/k - f_{c1}/k) \cdot e^{j\Phi_1} \cdot e^{-j(\pi/k)f^2}, \quad f \in \left[f_{c1} - \frac{B_1}{2}, f_{c1} + \frac{B_1}{2} \right]. \tag{2}$$

The reference function is then computed as the complex conjugate

$$H_{MF}(f) = W(f - f_{c1}) \cdot e^{j(\pi/k)f^2}. \tag{3}$$

A real weighting function $W(f)$ centered around the frequency (Doppler or range) centroid $f_{c1} = k \cdot t_c$ is imposed on the spectrum and determines the processed bandwidth $B_1 \leq k \cdot T_1$. Thus, after the inverse transform (again by employing the principle of stationary phase) and rectangular weighting (including W and a), the impulse response function (IRF) will be

$$f_1(t) = e^{j\Phi_1} \cdot e^{j2\pi f_{c1}(t-t_0)} \cdot \operatorname{sinc}[\pi B_1 (t - t_0)] \tag{4}$$

where sinc is the $\sin x/x$-function. The peak of the IRF (sinc function) will appear at position t_0, and the width of the mainlobe is a function of the integration time (bandwidth). The linear phase term in (4) is determined by the offset of the processed bandwidth of the baseband signal f_{c1}. This linear phase term is part of the focused SAR signal and cannot be removed without inserting undesired phase offsets into other focused IRFs at different positions. This linear phase term is illustrated in Fig. 1(a). The phase ramp of the three IRFs is the same. If a phase ramp of opposite sign would have been applied, centered to the middle target, the initial phase ramp would have been nulled but a position dependent phase offset would have been introduced into the other IRFs. Fig. 1(b) relates to the spectral analysis (SPECAN) case [19], which will be described in Section III.

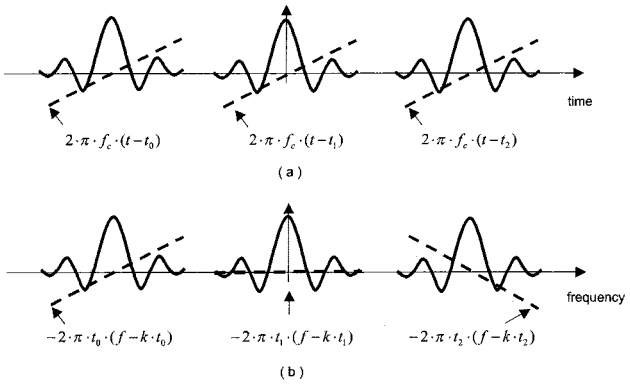

Fig. 1. Phase properties within the mainlobe of the SAR impulse response function for three targets for (a) stripmap focusing via matched filtering and (b) burst mode focusing with the SPECAN approach. The solid line gives the amplitude of the signal, and the dashed line the phase.

B. Coregistration Accuracy

Until now, the requirements on the coregistration accuracy have been determined by the constraint of keeping the coherence as high as possible [1], [20]. In [21], the effects of geometric misregistration were quantified, and it was shown that a phase bias due to misregistration will not appear in the final image, but the coherence will decrease according to a sinc function. It was found that a coregistration accuracy of 0.1 of the resolution cell is required to achieve high quality interferograms. However, the linear phase component within the mainlobe of the IRF has been neglected so far. Let us consider (4) to be the IRF of one channel of an interferometric pair obtained by matched filtering. The IRF of the second interferometric channel is obtained in a similar way

$$f_2(t) = e^{j\Phi_2} \cdot e^{j2\pi f_{c2}(t-t_0-\Delta t)} \cdot \operatorname{sinc}[\pi B_2 (t - t_0 - \Delta t)]. \tag{5}$$

There are three main differences between the two IRFs in (4) and (5). First, the signal phase is different in each case (first exponential term). Second, the center frequency values may be different but here we first assume that a common bandwidth is processed for both signals ($f_{c1} = f_{c2} = f_c$ and $B_1 = B_2 = B$). Third, there is a relative time shift (misregistration) between the two interferometric signals which is given by Δt. The effects of constant misregistration on the interferometric phase can be observed in Fig. 2. For perfect coregistration, the time shift Δt is zero, and the only resulting difference between the two signals is

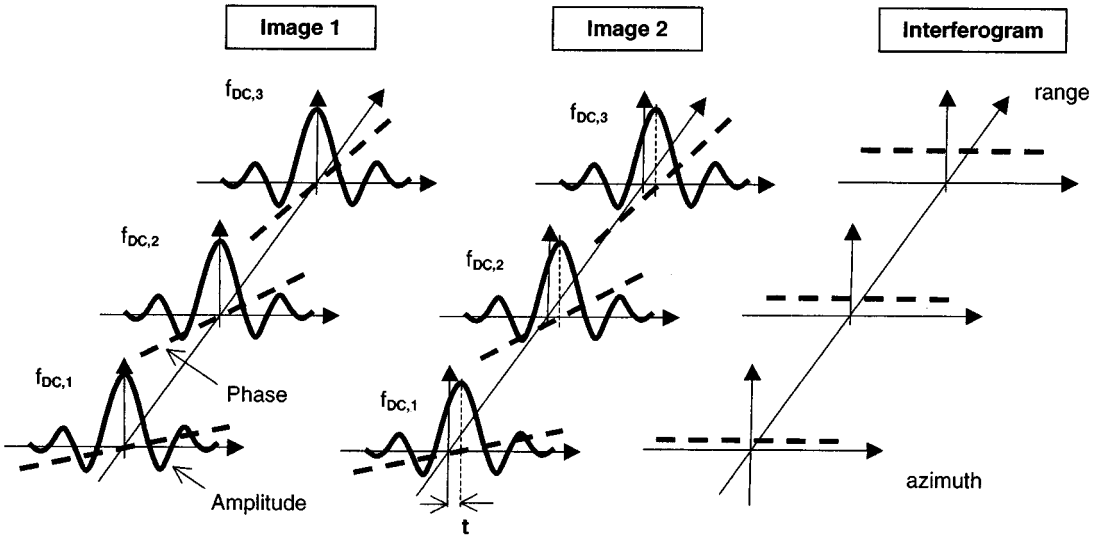

Fig. 2. Misregistered interferometric signal pair prior to interferogram generation. Range-dependent phase offsets occur due to misregistration, and the linear phase term of the IRF is imposed by the center frequency offset. When the center frequency is range dependent, the phase error due to misregistration is also range dependent.

the interferometric phase difference $\Phi_2 - \Phi_1 = 4\pi/\lambda \cdot (r_1 - r_2)$. It corresponds to the desired information on the terrain topography or displacement in the case of differential or along-track interferometry. In case of misregistration, an additional phase term will appear

$$\phi_{err} = 2\pi f_c \Delta t. \tag{6}$$

For a constant misregistation and constant center frequency f_c (i.e., constant Doppler centroid along range and azimuth), this error is constant and can easily be corrected using just one ground control point. In a practical case, this is not possible. First, the misregistration is often varying in range due to the imaging geometry and topography. Second, it can also vary in azimuth due to nonparallel orbits. Third, if SAR interferometry is performed with data of considerable squint, the azimuth focusing of the SAR processor accounts for variations of the squint over range in order to obtain good quality images with respect to SNR and ambiguity suppression. Thus, the linear phase term in (4) of the azimuth IRF becomes range dependent according to the Doppler centroid (f_c) variation. Note the phase ramp variation depicted in Fig. 2, which leads to a range dependent phase error according to (6).

Considering the RADARSAT system in stripmap mode with a yaw angle of 3°, an interferometric phase error of about 30° occurs from near to far range if the interferometric pair is misregistered by 0.1 sample in azimuth. This phase error leads to height errors greater than 25 m, assuming a horizontal baseline of 100 m. To reduce this systematic error to an acceptable level, an azimuth coregistration accuracy better than 0.01 samples is required. The use of several tiepoints, which is often required to precisely estimate the baseline, can only solve this problem for a small scene. For large imaged areas (i.e., several subsequent scenes) the squint variations in both range and azimuth must be accounted for and the tiepoint approach is not practical.

Such phase errors can also occur in the case of range misregistration due to the coupling of the range and azimuth signals for high squint angles. In this case, a range frequency centroid variation leads to similar effects as in azimuth [22]. These effects are more relevant to airborne SAR systems and have a smaller scale in the case of low and moderate topography. Therefore, they will not be detailed further here.

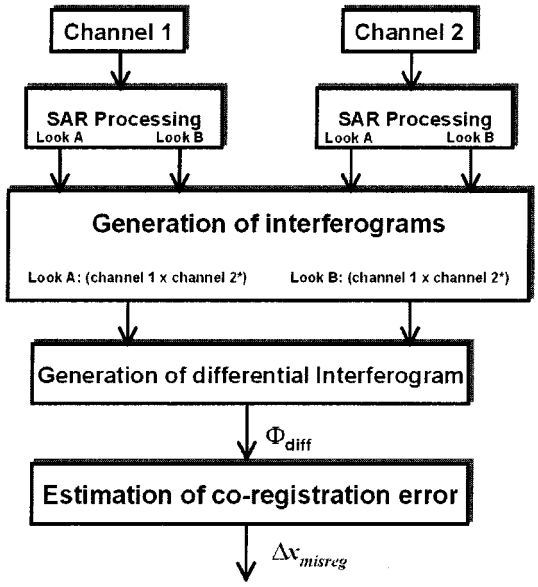

Fig. 3. Block diagram of the proposed spectral diversity approach for interferometric image coregistration.

C. Coregistration by Spectral Diversity

The basic idea of the proposed spectral diversity technique is to exploit the linear phase component given by the second exponential term of the IRFs in (4) and (5). The block diagram of the proposed method is presented in Fig. 3. First, the bandwidth of the full resolution SAR signals is separated into two parts (looks). This means that for each signal the spectrum is filtered

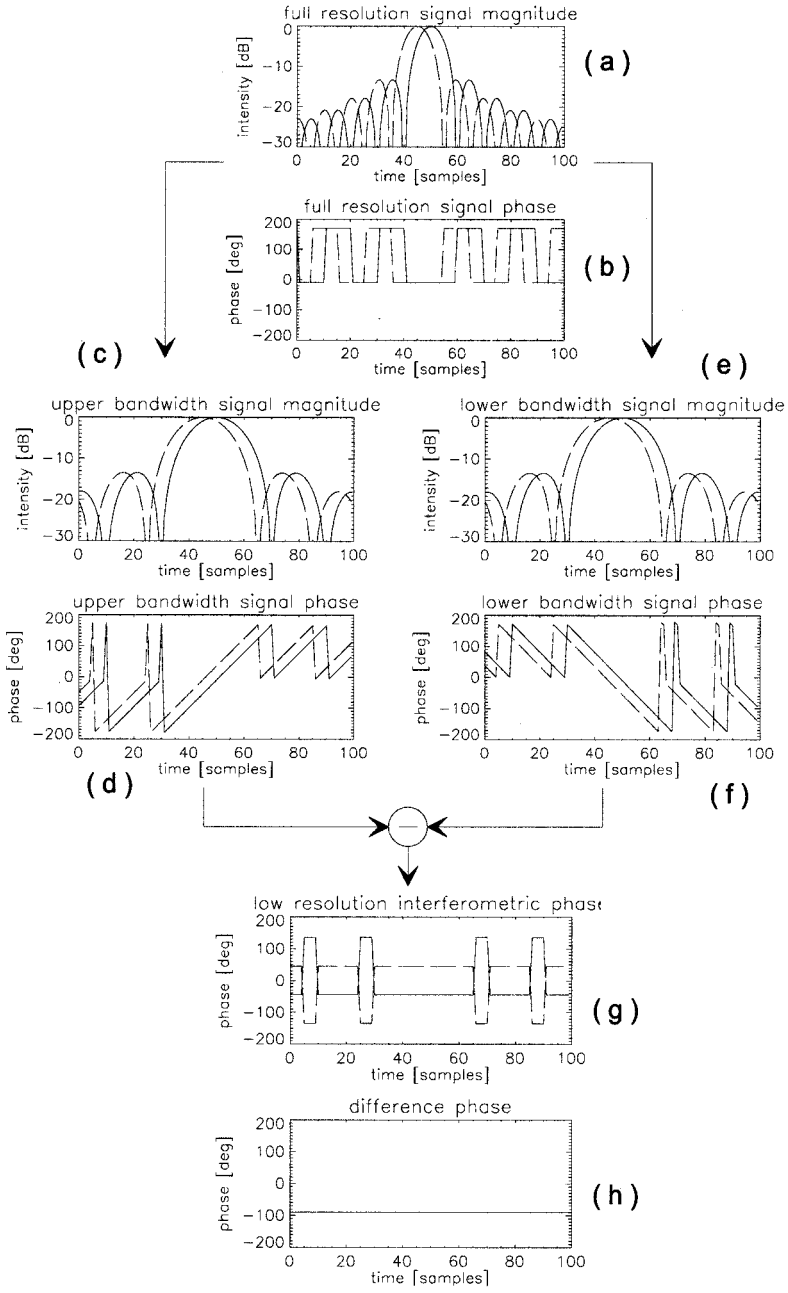

Fig. 4. Simulation of full resolution and bandfiltered signals for coregistration by spectral diversity. The solid line relates to the first interferometric channel and the dashed line to the misregistered second channel.

into two looks A and B, so that four IRFs f_1^A, f_1^B, f_2^A and f_2^B are obtained

$$f_1^A(t) = e^{j\Phi_1} \cdot e^{j2\pi f_c^A(t-t_0)} \cdot \mathrm{sinc}\left[\pi B_{look}(t-t_0)\right] \tag{7}$$

$$f_1^B(t) = e^{j\Phi_1} \cdot e^{j2\pi f_c^B(t-t_0)} \cdot \mathrm{sinc}\left[\pi B_{look}(t-t_0)\right] \tag{8}$$

$$f_2^A(t) = e^{j\Phi_2} \cdot e^{j2\pi f_c^A(t-t_0-\Delta t)} \cdot \mathrm{sinc}[\pi B_{look}(t-t_0-\Delta t)] \tag{9}$$

$$f_2^B(t) = e^{j\Phi_2} \cdot e^{j2\pi f_c^B(t-t_0-\Delta t)} \cdot \mathrm{sinc}[\pi B_{look}(t-t_0-\Delta t)] \tag{10}$$

where B_{look} is the filtered look bandwidth in range or azimuth. The indices 1 and 2 correspond to the channel number of the interferometric pair and the indices A and B to the different looks of the signal spectrum having different center frequencies f_c^A and f_c^B, respectively. In Fig. 4(a) and (b), the full resolution signals of (4) and (5) are displayed in terms of amplitude and phase. The signals are misregistered by five samples corresponding to half the resolution cell. For visualization purposes an oversampling by a factor of ten was chosen. The filtered bandwidth signals according to (7) and (9) are shown in Fig. 4(c) and (d), and according to (8) and (10) in Fig. 4(e) and (f), respectively. Both amplitudes and phases are represented. Note that the original sampling of the signals in these plots has not been changed

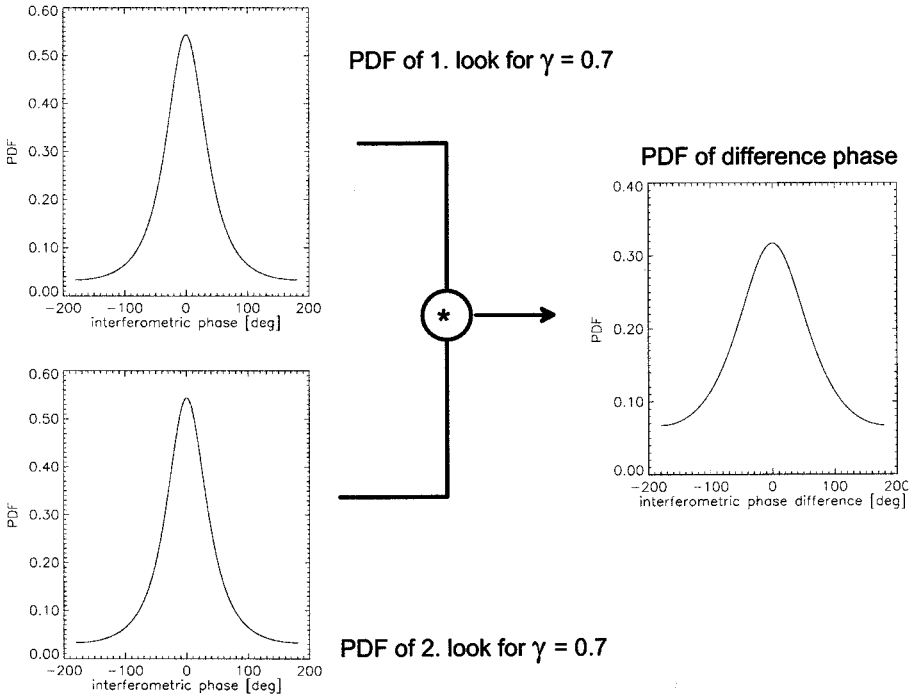

Fig. 5. Probability density function (PDF) of the difference phase as the convolution of the PDFs of the interferometric phase of the two looks.

even though the resolution of the looks is worse. The bandwidth of the full resolution signals is centered at frequency zero (no phase ramp within the mainlobe), whereas the spectral separation of the two looks is 50% of the total signal bandwidth and is symmetric about zero. This induces phase ramps of opposite signs within the mainlobe of the two low resolution signals [see Fig. 4(d) and (f)]. The filtered bandwidth of each signal is 50% of the bandwidth of the full resolution signals.

In Fig. 4(g), the interferometric phase of each interferometric look is shown to be constant within the mainlobe according to (6). Finally, their difference phase gives the estimate of the coregistration error according to

$$\Delta t = \frac{\phi_{diff}}{2\pi(f_c^A - f_c^B)} \tag{11}$$

where ϕ_{diff} is the measured phase difference of the two interferograms [see Figs. 3 and 4(h)]. Equation (11) shows that the absolute value of the selected center frequencies of the two looks is not relevant. Only the relative difference $(f_c^A - f_c^B)$ is used for the determination of the coregistration error between the two images. The looks should not overlap, and a weighting for sidelobe suppression is recommended. It must be emphasized that the whole procedure is computationally very effective assuming that the complex looks can be generated during the processing. In any case, no cross correlations or interpolations are required.

D. Algorithm Accuracy

The accuracy investigations performed here are based on the assumption that the received SAR signals can be described as circularly random Gaussian processes. It was shown in [21] that the probability density function (PDF) of the single-look interferometric phase ϕ can be expressed as a function of the correlation coefficient (or coherence magnitude) γ of the interferometric pair

$$\mathrm{PDF}(\phi) = \frac{1-\gamma^2}{2\pi} \cdot \frac{1}{1-\gamma^2 \cdot \cos^2 \phi} \cdot \left[1 + \frac{\gamma \cdot \cos \phi \cdot \arccos(-\gamma \cdot \cos \phi)}{\sqrt{1-\gamma^2 \cdot \cos^2 \phi}}\right]. \tag{12}$$

The interferometric phase ϕ in this equation is restricted to the interval $[-\pi, \pi]$. Assuming further that the two looks used for the proposed method are statistically independent (in case of nonoverlapping looks, this is the case), the PDF of the interferometric phase difference can be evaluated as the convolution of the PDFs of the two interferometric looks. We performed this evaluation numerically, and the result for $\gamma = 0.7$ and no sample averaging is shown in Fig. 5. The broadening of the phase distribution indicates an increase of the standard deviation of the phase difference when compared to the single-look phase of one interferogram, which is displayed in Fig. 6. Equation (11) gives the relation to the standard deviation of the estimated coregistration error. Thus, the accuracy of the misregistration estimate is strongly influenced by the correlation coefficient γ of the interferometric pair, which is a function of the SNR (backscatter), the baseline separation, the possible misregistration, and temporal changes [3]

$$\gamma = \gamma_{\mathrm{SNR}} \cdot \gamma_{spatial} \cdot \gamma_{misreg} \cdot \gamma_{temporal}. \tag{13}$$

To reduce the noise of the difference phase, it is important to keep all coherence contributions as high as possible. The terms accounting for the SNR and for the temporal decorrelation (γ_{SNR} and $\gamma_{temporal}$) cannot be improved, but the spatial (baseline) decorrelation ($\gamma_{spatial}$) should be eliminated by

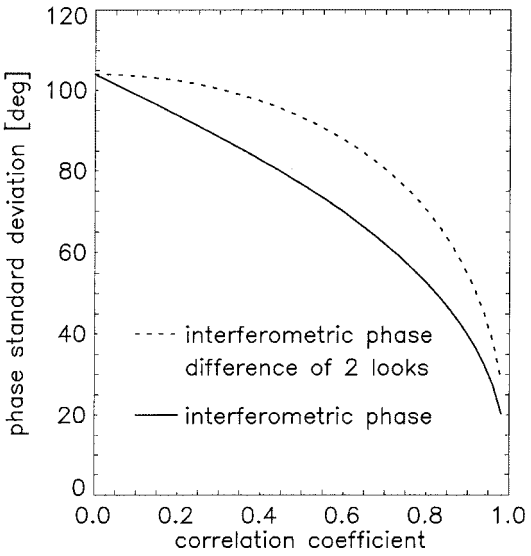

Fig. 6. Standard deviation of the interferometric phase and of the interferometric phase difference as a function of the correlation coefficient.

means of spectral shift filtering [23]. Also, the misregistration term (γ_{misreg}), which behaves like a sinc function [21], should be reduced as much as possible before the spectral looks are combined, for example by an *a priori* coregistration of the two interferometric images to one sample accuracy. In fact the generation of the low bandwidth looks also reduces the misregistration noise to a great extent.

Example: For $\gamma = 0.7$ the expected standard deviation of the difference phase with no sample averaging is 80°. Then, for a spectral separation of the looks of half the sampling frequency f_s, the standard deviation of the misregistration estimate becomes a 0.45 sample. An accuracy of 0.01 sample can be obtained by spatial averaging over a window of ca. 50×50 resolution cells. Due to the oversampling of the two one-look interferograms, this corresponds to about four times more samples (i.e. 100×100 samples).

E. Accuracy Assessment on Real Data

We have tested the accuracy of the proposed coregistration approach on real E-SAR data (the same data are used in Section IV), and we have compared it with the accuracy obtained by the conventional cross-correlation method.

The commonly used multilook filter [1], [24] was first used to average the interferometric phase difference, taking into account the signal amplitude. But we found that the same filter applied to the normalized complex image samples leads to a much better standard deviation. We explain this by the reduced influence of strong scatterers with non-corner reflector-like behavior. Similar conclusions were also taken in [25], [26]. Furthermore, we found that a maximum look separation and largest nonoverlapping look bandwidth lead to the best performance of the proposed method. This is obvious since a large look bandwidth allows more independent samples to be averaged, and a large look separation reduces the noise of the measured difference phase according to (11). In case of overlapping looks, we found that the misregistration will be underestimated depending on the amount of spectral overlap and the imposed weighting values.

We have obtained a standard deviation of 0.04 sampled (measured over individual estimates over range) by averaging 2048 full resolution complex azimuth samples. The same accuracy was obtained when using the well known cross-correlation method with an oversampling of 32 for the correlation peak. Theoretical investigations and a simulation on the accuracy of the cross-correlation method can be found in [27], [28].

III. ScanSAR Image Coregistration

Basically, ScanSAR imaging exploits a scanning strategy of the antenna in elevation in order to enlarge the swath coverage during one overflight. This is done at the expense of azimuth resolution because the synthetic aperture of the antenna must be shared with several subswaths. The short azimuth illumination time for each subswath arises from a series of received radar echoes which are commonly denoted as a burst.

ScanSAR interferometry has recently been demonstrated to be feasible with RADARSAT data [29]. Due to the large swathwidth, ScanSAR interferometry has great potential for global coverage with increased revisit times. Also, the combination of one ScanSAR and one stripmap SAR image was shown to be suitable for interferometry [29], [30]. In this section, the indispensable azimuth coregistration of the ScanSAR image pairs will be discussed and a solution will be presented based on the spectral diversity technique presented in Section III.

A. Azimuth Focusing by Spectral Analysis

The SPECAN approach is commonly used to produce SAR images at medium or low resolutions [19]. It is very attractive in the case of ScanSAR and Spotlight [31] imaging. The SPECAN approach requires only one FFT to focus the SAR image in the azimuth direction. This leads to an azimuth image representation in the frequency domain, whereby the azimuth image geometry is related to the time domain by the modulation rate $k = f/t$. Although the calculations for the SPECAN approach are different from the matched filter case, they lead to a similar result. First, the signal in (1) is deramped with a complex conjugate reference signal

$$h_{SP}(t) = w(t) \cdot e^{-j\pi k t^2}. \tag{14}$$

For simplicity, $w(t)$ is considered to be a rectangular weighting of length T_1 centered around $t = 0$. After spectral analysis, the focused signal is

$$F_{1,\,Specan}(f) = e^{j\Phi_1} \cdot e^{j(\pi/k)f_{c1}^2} \cdot \mathrm{sinc}\left[\pi T_1 \left(f - f_{c1}\right)\right] \tag{15}$$

i.e. the IRF peak appears at position $f_{c1} = k \cdot t_0$, and will have a constant phase offset [second exponential term in (15)] depending on its position. In order to assure a phase preserving response for all focused IRFs a quadratic phase correction function

$$\phi_{corr} = -\frac{\pi}{k} \cdot f^2 \tag{16}$$

should be applied to cancel out correctly this constant phase term for each azimuth position. Thus, the following expres-

sion is obtained after regrouping the linear and quadratic phase terms:

$$F_{1,Scan}(f) = e^{j\Phi_1} \cdot e^{-j(\pi/k)(f-f_{c1})^2} \cdot e^{-j2(\pi/k)f_{c1}(f-f_{c1})} \cdot \operatorname{sinc}\left[\pi T_1 (f - f_{c1})\right]. \quad (17)$$

For the peak position all phase terms except the first one (signal phase) vanish. The second quadratic phase term can be considered negligible within the mainlobe of the IRF, but the third linear phase term is important. Note that the slope of the phase in this case depends on the position of the focused mainlobe. It is important to understand the difference of this effect compared to matched filter focusing in the stripmap case, as it is of concern for the investigation of the azimuth misalignment in ScanSAR interferometry. For comparison, the phase behavior for the matched filter and SPECAN focusing are depicted in Fig. 1. In the case of the stripmap imaging with matched filtering all targets are focused at the same center frequency whereas in case of ScanSAR acquisition each target is focused at a different center frequency, which leads to different phase slopes depending on the IRF position. A derivation of the IRF for ScanSAR imaging based on the matched filter principle leads to the same results (see for example [32]) as presented here for the SPECAN approach.

B. ScanSAR Azimuth Coregistration Accuracy

Based on the above considerations, the azimuth coregistration problem in ScanSAR interferometry is investigated. Consider a focused ScanSAR azimuth signal according to (17) and its interferometric pair, which is slightly misregistered by Δt

$$F_{2,Scan}(f) = e^{j\Phi_2} \cdot e^{-j(\pi/k)(f-f_{c1}-\Delta f)^2} \cdot e^{-j2(\pi/k)f_{c1}(f-f_{c1}-\Delta f)} \cdot \operatorname{sinc}\left[\pi T_1 (f - f_{c1} - \Delta f)\right] \quad (18)$$

with $\Delta f = \Delta t \cdot k$, where k is the Doppler rate. The resulting interferometric ScanSAR phase for the IRF position will be

$$\Phi_{\mathrm{ScanSAR}} = (\Phi_2 - \Phi_1) + 2\pi f_{c1}\Delta t. \quad (19)$$

Note that within a burst this corresponds to a superposition of the desired interferometric component with a linear phase term, since f_{c1} is a function of the azimuth position within the burst. Note also that this effect can be much stronger than the interferometric phase. For example, a misregistration of one raw data sample ($\Delta t = 1/f_s$, f_s is the pulse repetition frequency (PRF), which corresponds to much less than 0.1 of a ScanSAR azimuth resolution cell, introduces a ramp of 2π within each burst, assuming the complete variation of f_{c1}, $f_{c1} \in [-f_s/2, +f_s/2]$. Therefore, we state that the burst coregistration must be more accurate than 0.01 raw data samples in order to ensure negligible phase errors. The algorithm presented in Section II is able to efficiently achieve the accuracy requirement also in the ScanSAR case after some modifications.

C. Spectral Diversity for ScanSAR Azimuth Coregistration

Basically, ScanSAR data can be processed in different ways. In the case of using standard strip mode processors (i.e. matched filtering) [33], [34], zero padding between the bursts of each subswath must be performed and thus the processing becomes inefficient. In this case, also the coherent azimuth looks cannot be directly accessed. Instead, if the processing is performed burst by burst, efficient SPECAN techniques can be used and the different azimuth looks are directly available [17], [32]. For each raw data burst, one image look is generated. Its azimuth size in terms of valid samples is determined by the synthetic aperture minus the length of one raw data burst. For subsequent raw data bursts, these image looks are overlapped. Since they are related to different azimuth squint angles, they can be used for multilooking [13].

Two azimuth looks of ScanSAR data are used to illustrate the azimuth coregistration method for ScanSAR processing. The spectral diversity technique described in Section II can easily be modified if the IRFs [(4) and (5)] of the stripmap case are compared to those of the ScanSAR SPECAN case ((17) and (18)). The most important modification is because the center frequencies of the looks f_c^A and f_c^B are now a function of the azimuth time and range position t and r. Therefore, (11) changes to

$$\Delta t = \frac{\phi_{diff}}{2\pi(f_c^A(t, r) - f_c^B(t, r))}. \quad (20)$$

The phase variation of each one look interferogram is nearly linear in azimuth ($f_c = k \cdot t$), while the variation in range depends on the Doppler centroid and Doppler rate behavior over range. Note that this method is very effective since the different azimuth looks are directly available, in contrast to the stripmap case, where extra look generation is often required. In order to avoid decorrelation in ScanSAR interferometry, a part of the samples within each raw data burst of the interferometric pair must be discarded [34], [29]. This ensures that the processing is performed with roughly the same Doppler centroid for each image. After the correct misregistration parameters are found, the azimuth shifts must be performed on the raw data of one channel before invalid range lines are discarded, and this image must then be reprocessed. The example given in Section IV-B will further detail the implementation aspects in the ScanSAR case.

IV. Experimental Results

This section presents two coregistration examples using the proposed technique with real SAR data. In the first case, airborne data is used to demonstrate a two-dimensional (2-D) coregistration case for repeat-pass SAR interferometry while in section B, the azimuth coregistration for ScanSAR data is demonstrated.

A. Airborne Repeat-Pass Interferometry

Airborne SAR data acquisition is affected by motion errors that must be corrected during raw data processing. Especially in the repeat-pass case and when interferometric tracks are acquired with an unstable platform like the E-SAR aircraft, a DO-228 [35], [12], the required accuracy for coregistration often cannot be met due to limitations of the inertial system or unfavorable GPS configuration. A precise coregistration procedure can overcome these limitations, making the data usable e.g. for investigation of coherence changes, volume

TABLE I
PARAMETERS OF THE E-SAR SYSTEM IN L-BAND FULL POLARMETRIC IMAGING MODE

parameter	typical value
operating frequency	1.3 GHz
range bandwidth	50 or 100 MHz
chirp duration	5 μsec
sampling rate	60 or 100 MHz
PRF	400 Hz/channel
forward velocity	89 m/s
flight altitude	3000 m
incidence angle	20-60 deg

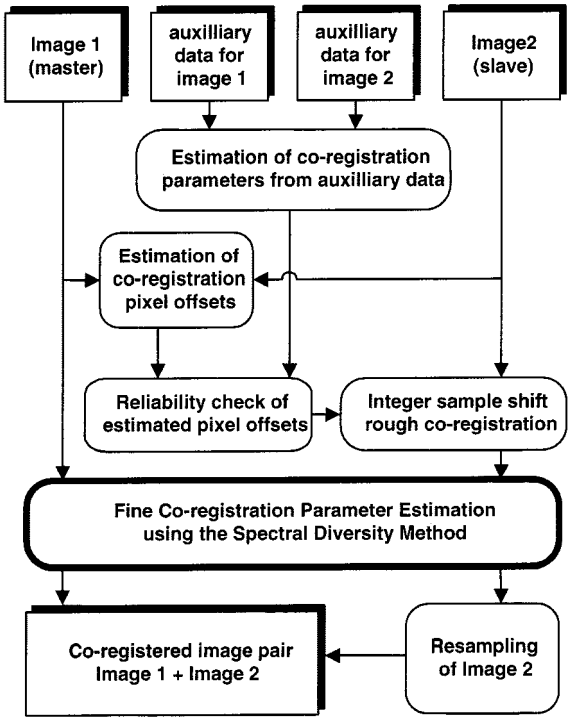

Fig. 7. Strategy for coregistration of repeat-pass interferometric data.

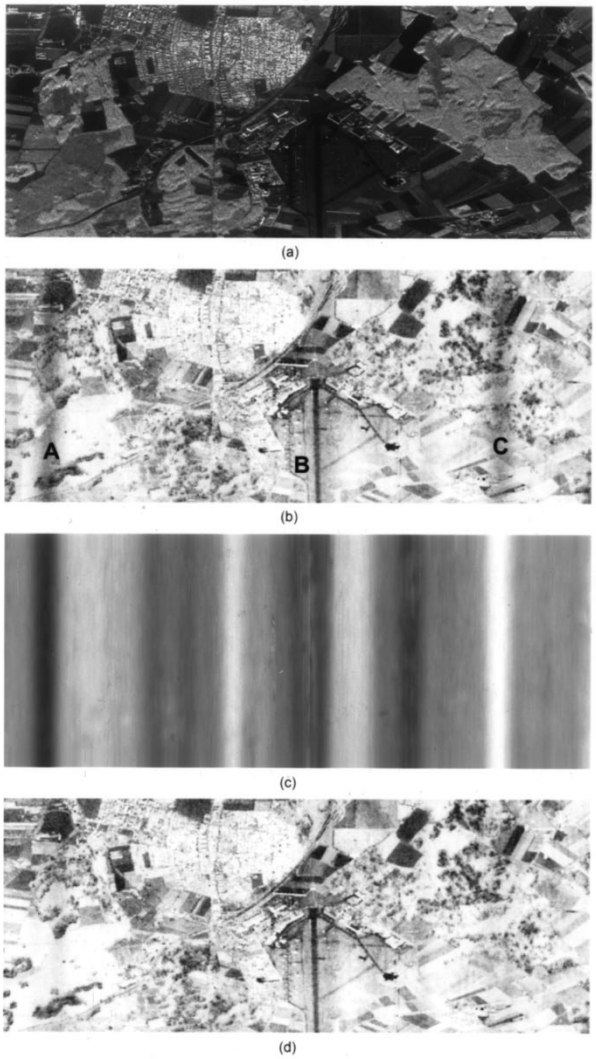

Fig. 8. E-SAR image of Oberpfaffenhofen airfield. (a) L-band, HH-polarization, 4-look intensity image. (b) Coherence map for a 15 min repeat-pass pair. Resampling according to misregistration information based on conventional methods. (c) Azimuth misregistration variations, scaled to ± 1.5 samples, as measured by the spectral diversity method. (d) Coherence map for the same data pair, but resampled according to the information from (c).

decorrelation, or for polarimetric interferometry [36]. Relevant parameters for the E-SAR data used in this example are summarized in Table I. The spectral diversity coregistration technique of Section II has been applied to the full polarimetric L-band repeat-pass data of the E-SAR system. According to the block diagram of Fig. 7, the preliminary coregistration offsets are computed on a block-by-block basis either from the navigation data itself or by simple cross correlation. In this way, the integer pixel offsets in the range and azimuth directions are found and corrected. In a second step, the proposed technique is applied in both the range and azimuth directions with the following parameters.

1) *Look Bandwidth*: one-third of the full resolution bandwidth.
2) *Look Separation*: one-third of the full resolution bandwidth. The look separation is not the maximum possible. This is to avoid the wrapping of the difference phase in case of large variations of the misregistration within a small area.
3) *Window Size for averaging*: 20×80 full resolution samples.
4) *Coherence Threshold*: 0.6. Only those regions of the interferogram with a coherence higher than this limit are used for the coregistration estimate.

The results in Figs. 8–10 present the improvements due to the new method. Fig. 8(a) depicts the 4-look L-band HH polarized intensity image of an area of 8 km (azimuth) $\times$ 3.5 km (range) around Oberpfaffenhofen, including the DLR facility and the airfield. The image resolution is 3 m in azimuth and 2 m in slant range. Fig. 8(b) is the coherence map for the HH-polarized repeat-pass interferogram with a revisit time of 15 min. The

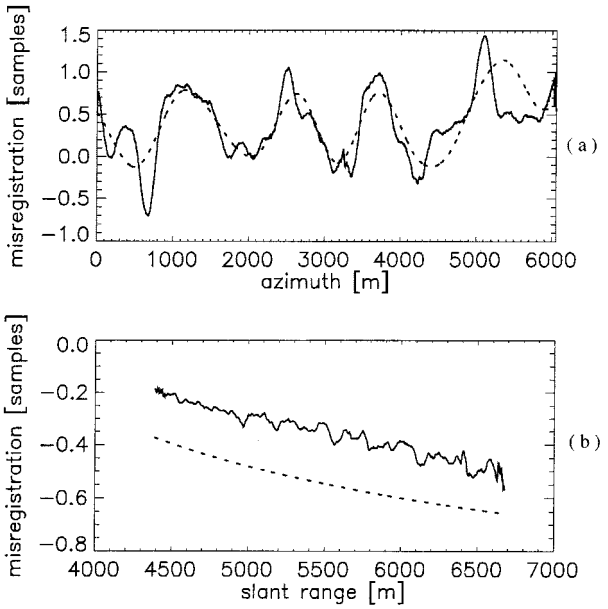

Fig. 9. (a) Estimated azimuth misregistration using the spectral diversity technique and a conventional method (dashed line). (b) Estimated range misregistration and theoretical values (dashed line) according to the measured tracks.

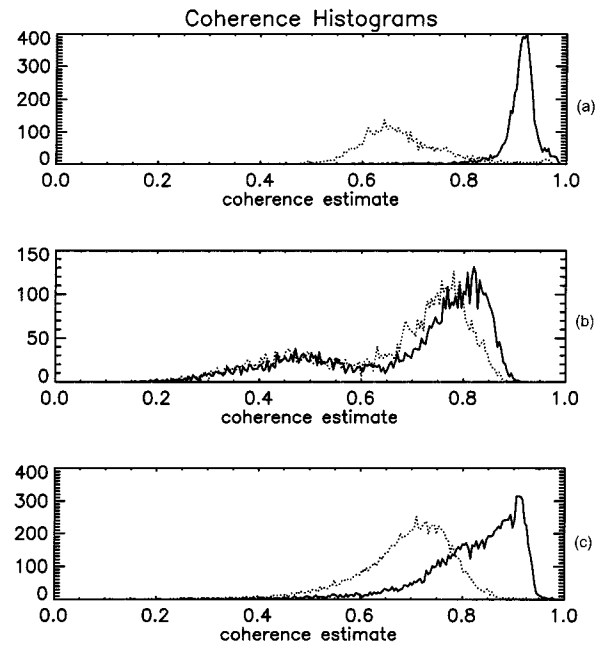

Fig. 10. Coherence improvement on three selected areas: (a) according to the area A in image 8(b), (b) area B near the runway, and (c) according to area C in image 8(b).

mean effective baseline for this image pair was ca. 1 m. This coherence map was obtained after coregistration of the interferometric pair with the operational strategy for processing the repeat-pass E-SAR data. It employs a conventional coherence optimization scheme working on ten blocks of azimuth data. The values between the blocks were evaluated by cubic spline interpolation. The coherence map shows that this algorithm did not lead to a satisfactory result because the update and accuracy of the azimuth misregistration estimates is not high enough. In Fig. 8(c), the measured azimuth misregistration using the proposed spectral diversity technique is presented. The grey values are scaled to ± 1.5 samples of misregistration. The new coherence map after resampling the second image with this information is depicted in Fig. 8(d). The dark coherence stripes of Fig. 8(b) disappeared when resampling with the accurate coregistration results.

Fig. 9(a) presents the comparison of the azimuth misregistration estimates obtained with the conventional coherence optimization method (dashed line) and those of the proposed spectral diversity technique. Note that the new technique is able to measure even rapid changes of the coregistration errors correctly, which exactly relate to the low coherence areas of Fig. 8(b). In these areas, the conventional method failed. In fact, it suffers from undersampling and four times more blocks (in that case, with overlap to ensure the required accuracy) would have been required.

The estimated coregistration error in the range direction is presented in Fig. 9(b). In this case, the approximately linear behavior of the misregistration, which is naturally imposed by the different imaging geometry, has correctly been measured. For comparison the estimated coregistration values calculated from the measured tracks are displayed (dashed line). The offset to be observed relates to the inaccuracy of the kinematically processed differential GPS data of the two tracks which is in the order of 10–20 cm for each track.

Three areas (corresponding to the positions of largest difference between the azimuth coregistration estimates) were selected for analysis: A was the low coherence area in the left part of Fig. 8(b), B was the area around the runway, and C was the low coherence area in the right part of Fig. 8(b). The coherence improvement can be seen by comparing Fig. 8(b) and (d). The corresponding coherence histograms are shown in Fig. 10(a)–(c), respectively. The region of the histogram in Fig. 10(b) with a coherence between 0.4 and 0.6 could not be improved by the accurate coregistration estimates since it arises from the low reflectivity values of the runway in the image.

B. ScanSAR Interferometry

The ERS tandem pair: ERS-1, orbit 23299, frame 2637–ERS-2, orbit 03626, frame 2637, covering a part of Austria in the vicinity of Vienna has been selected to simulate a ScanSAR image pair using one subswath out of five. The parameters for the simulation were: 39 valid azimuth samples plus nine unvalid samples per burst, making a total of 240 samples per burst cycle, and four complete burst cycles per synthetic aperture. 50 bursts were processed to generate an image with four complex azimuth looks which were stored in separate files. The azimuth image sampling was set to 88.95 m and a total of 46 valid samples are stored for each image look. The corresponding azimuth frequency vectors, which relate to the center frequencies of different azimuth positions within a burst, have also been stored in order to be available for the subsequent coregistration scheme. The extended chirp scaling algorithm (ECSA) for ScanSAR data [17] has been employed to process the raw data bursts individually. The advantage is that it is phase preserving, and it allows easy access to the different azimuth looks. Precise orbit information was used to determine

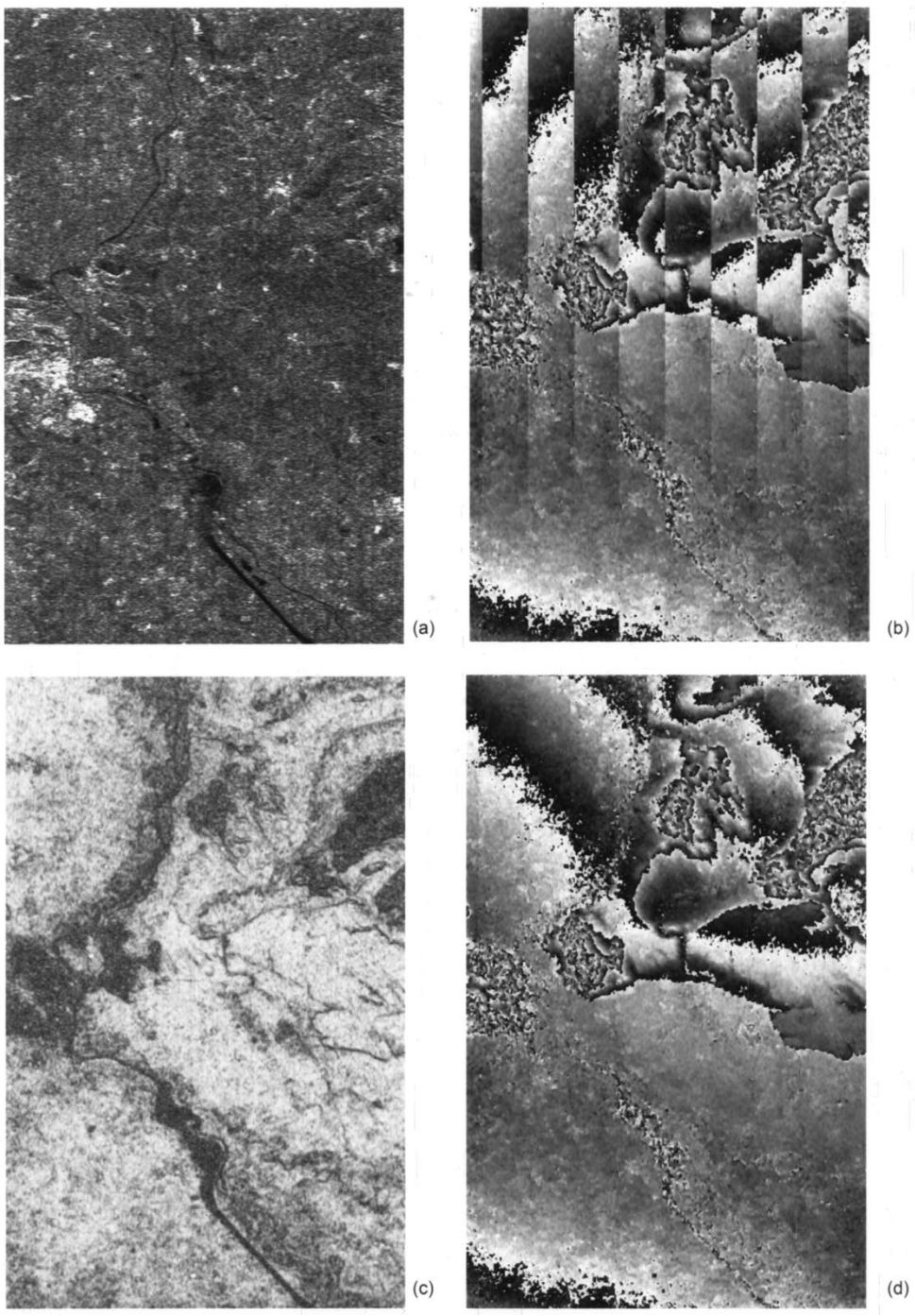

Fig. 11. Simulated ScanSAR data based on an ERS tandem pair (azimuth is horizontal, range vertical). (a) Intensity image processed to four azimuth looks and six range looks. (b) Interferometric phase of one azimuth look with inaccurate burst alignment (eight complete bursts are shown). (c) ScanSAR coherence map. (d) Interferometric phase of one azimuth look after accurate azimuth coregistration.

the initial azimuth and range integer pixel offsets prior to the extraction of the raw data bursts. Spectral shift filtering [23] has been performed during processing according to the mean effective baseline of 240 m, and range coregistration has been assured by a relative constant shift plus a linear stretch of one image. Therefore, we used the range scaling properties of the ECS algorithm [17].

Fig. 11(a) presents eight complete bursts of the processed image with an extension of ca. 36 km in azimuth and 62 km in slant range. The River Danube crosses the scene vertically. The four azimuth looks are superimposed. Thus, the scalloping is reduced. The number of range looks is six. The interferometric phase of the first look after subtraction of the dominant component due to flat Earth is shown in Fig. 11(b). According to (19), a strong linear phase is overlayed on the topographic information within each burst, making any further phase evaluation impossible. This effect is due to a residual (range dependent because of slightly nonparallel orbits) azimuth misregistration. It was shown in Section III that a misregistration of one raw data sample, corresponding to 0.05 of a ScanSAR image sample (one

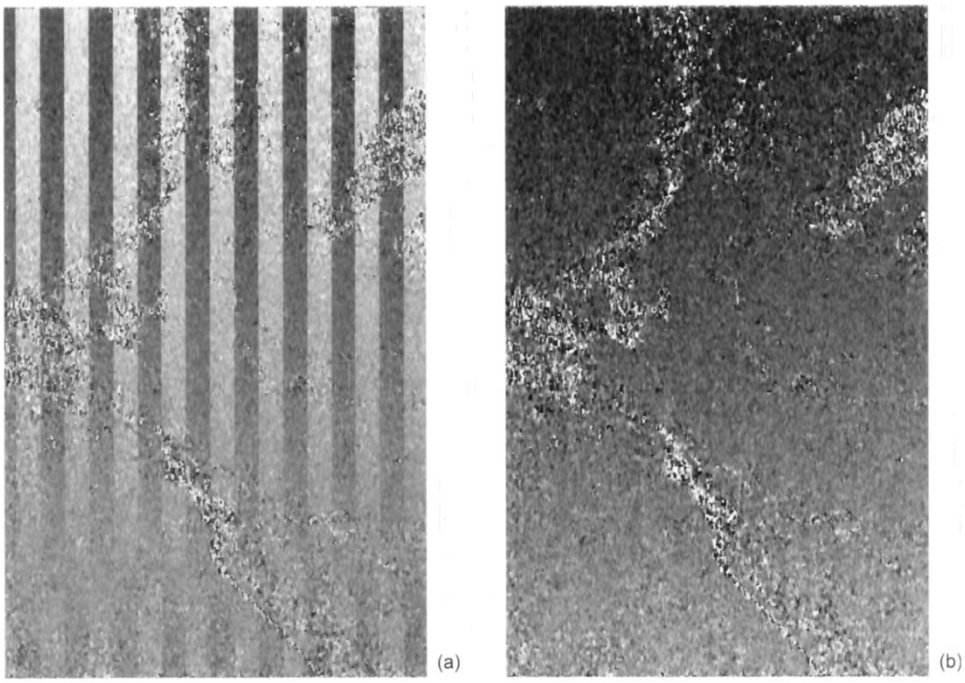

Fig. 12. (a) Difference phase map between the first and third azimuth look. (b) Estimated azimuth misregistration map scaled to ± 1 azimuth raw data sample.

image sample is 88.95 m in our example), induces a linear ramp of 360° within each burst (less if invalid samples are discarded). Note that this misregistration does not affect the coherence estimate noticeably, which is depicted in Fig. 11(c). The proposed spectral diversity technique adapted for ScanSAR data is very suitable for measuring this small coregistration error. The corrected interferometric phase is shown in Fig. 11(d) for the first azimuth look.

The operation of the alignment algorithm is presented in the Figs. 12 and 13. Fig. 12(a) shows the interferometric phase difference between the first and the third azimuth look. The stripes in Fig. 12(a) are along the range direction and arise twice as frequently as in the image interferogram of look one [compare with Fig. 11(b)]. This is due to the fact that the first and third look interferograms (which form the difference interferogram) are shifted by approximately half an image look's length. This shift arises from the ScanSAR scanning strategy. A sliding window of 20 has been applied only in the range direction of both complex look interferograms, and the complex difference interferogram has also been filtered in a similar way. This difference phase is used in (20) and the resulting estimate of the azimuth misregistration is depicted in the grey scale of Fig. 12(b), scaled to ± 1 raw data sample (i.e. ± 4.2 m). The areas with a noisy phase correspond to areas of coherence lower than 0.6 and are not considered for coregistration estimation.

Fig. 13(a) shows the values of the azimuth frequency vectors for the first and third look, to which each image look point is focused. For each burst, they are centered around the common Doppler centroid (i.e., 342 Hz). The frequency difference is shown in Fig. 13(b). It jumps appear at the borders of the bursts and exactly match the phase jumps of the difference interferogram in Fig. 11(a). Fig. 13(c)–(e) presents one single azimuth line (line 3450 of a total of 3780 of the selected ERS-1/2 images) and show the difference phase [according to Fig. 12(a)], the measured misregistration [according to Fig. 12(b)], and the coherence [according to Fig. 11(c)], respectively. The regions of distorted misregistration estimates correspond to areas of low coherence [compare Fig. 13(d) and (e)] and are not used in the final estimation. To also assure the correct spectral alignment, the coregistration was then performed at the raw data stage of the second ScanSAR image according to the shift estimated by the proposed technique. The shift was considered constant over azimuth and its variation over range has been found by complex averaging the difference phase estimates over 20 range samples and 350 azimuth image sample. Samples of coherence less than 0.6 were excluded from the averaging. The standard deviation of our estimate was found to be 0.007 raw data samples (ca. 3 cm). It can further be improved if one considers that a total of six different look combinations can be used in this four azimuth look example.

V. Discussion

The proposed technique for estimation of the misregistration between interferometric pairs has been validated for stripmap and ScanSAR imaging modes. It can be applied in both the range and azimuth directions, and the estimates are made on a pixel by pixel basis. Due to the low pass characteristic of the coregistration error, pixel averaging is used to increase the accuracy of the estimation. The advantages compared to conventional coregistration techniques are twofold. First, the proposed technique can more efficiently track rapid changes of the coregistration errors, as demonstrated for the repeat-pass airborne case. Since the misregistration is estimated on a pixel-by-pixel basis, no interpolation and cross-correlation procedures, nor coherence or fringe optimization, must be performed. Second, in the azimuth ScanSAR case, the technique is extremely efficient

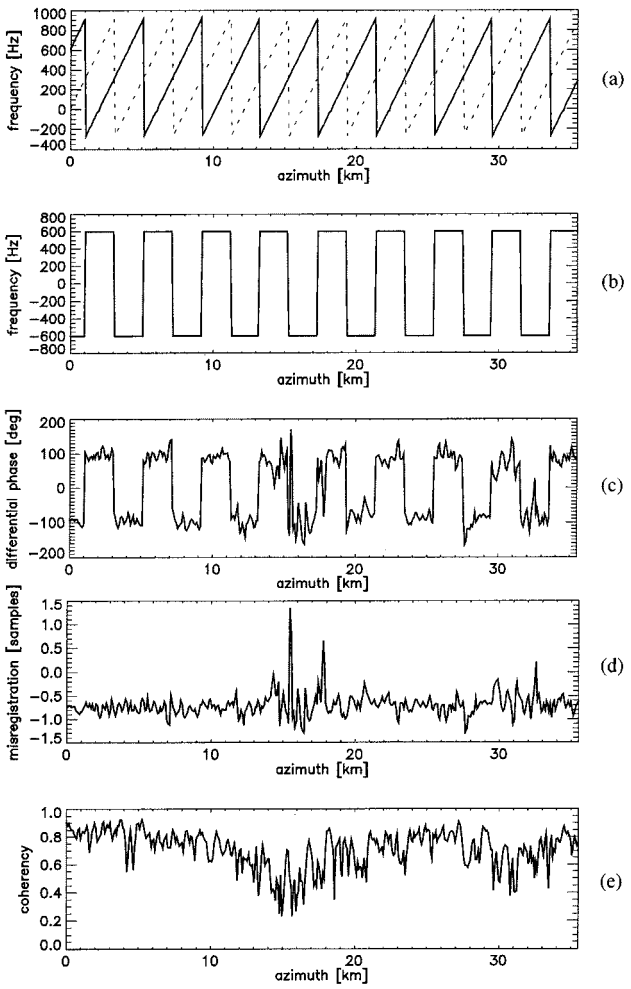

Fig. 13. (a) Azimuth frequency vector for look 1 (solid line) and look 3 (dashed line) of the simulated ScanSAR operation mode. (b) Frequency difference (look separation) as a function of azimuth position. (c) Difference phase between look 1 and 3 [horizontal cut through Fig. 12(a)]. (d) Estimated raw data burst misalignment [horizontal cut through Fig. 12(b)]. (e) Coherence information [horizontal cut through Fig. 11(c)].

since it makes use of the complex looks, which are readily available according to each burst being processed. Furthermore, the implementation of the method is very simple, and it has been demonstrated that it is able to precisely perform the difficult task of coregistration of the azimuth bursts.

The requirements on coregistration accuracy have been reconsidered in this paper. For high squint angles and for burst mode SAR imaging like ScanSAR, the accuracy requirement is much higher than the requirements defined so far in the SAR literature for stripmap SAR interferometry. In the case of ScanSAR interferometry simulated from ERS-1/2 data, we could achieve an accuracy of 0.007 samples (3 cm) by averaging ca. 20 (range) $\times$ 350 (azimuth) image samples. This leads to a residual linear phase ramp of ca. 2.5° within the burst length, which corresponds to less than one meter topographic height error in the simulated ScanSAR case of ERS-1/2.

While the high requirements for ScanSAR coregistration can be achieved by the proposed technique, very high squint angle SAR imaging can pose a limiting factor for SAR interferometry. A very small coregistration error can lead to phase errors of several multiples of 2π. In this case, one should first apply a very small look frequency separation and then increase it step by step. This procedure is able to solve the problem posed by the unknown ambiguity number of the estimated difference phase. When increasing the look frequency separation, the accuracy of the misregistration estimation is improved as well.

The proposed technique can also be used for range coregistration of a two frequency SAR interferometric system [8], whereby the two different frequency channels can directly be used as the range looks required to form the difference interferogram. However, if the frequency separation between the two channels is very large, the difference phase may become ambiguous even in the case of small coregistration errors. This problem can be circumvented by first applying the proposed technique to range looks generated within the available bandwidth of each frequency channel. Then, the different frequency channels can be used for increasing the coregistration accuracy.

Future work will include the investigation of this technique for coregistration error estimation applied to airborne SAR interferometry with very high squint angles and also for Spotlight SAR interferometry [31].

ACKNOWLEDGMENT

The authors would like to thank their colleague, J. Mittermayer, for useful discussions and for providing the ScanSAR processing routine. They would also like to thank the anonymous reviewers for their comments and suggestions.

REFERENCES

[1] F. Li and R. Goldstein, "Studies of multibaseline spaceborne interferometric synthetic aperture radars," *IEEE Trans. Geosci. Remote Sensing*, vol. 28, pp. 88–97, Jan. 1990.

[2] A. K. Gabriel, R. M. Goldstein, and H. Zebker, "Mapping small elevation changes over large areas: Differential radar interferometry," *J. Geophys. Res.*, vol. 94, no. B7, pp. 9183–9191, 1989.

[3] R. Bamler and P. Hartl, "Synthetic aperture radar interferometry," *Inv. Probl.*, vol. 14, no. 1, pp. R1–R54, 1998.

[4] A. K. Gabriel and R. M. Goldstein, "Crossed orbit interferometry: Theory and experimental results from SIR-B," *Int. J. Remote Sensing*, vol. 9, no. 5, pp. 857–872, 1988.

[5] Q. Lin, J. Vesecky, and H. Zebker, "New approaches in interferometric SAR data processing," *IEEE Trans. Geosci. Remote Sensing*, vol. 30, pp. 560–567, May 1992.

[6] S. Madsen, "On absolute phase determination techniques in SAR interferometry," in *Proc. SPIE*, vol. 2487, Apr. 1995, pp. 393–401.

[7] W. Xu *et al.*, "Phase unwrapping of SAR interferogram with multi-frequency or multi-baseline," in *Proc. IGARSS*, Pasadena, CA, 1994, pp. 730–732.

[8] C. Fischer, K. Schmitt, and W. Wiesbeck, "3-D interferometric SAR algorithm for discontinuous distributed objects," in *Proc. IGARSS'99*, Hamburg, Germany, June 1999.

[9] A. Moreira and R. Scheiber, "A new method for accurate co-registration of interferometric SAR images," in *Proc. IGARSS'98*, July 1998.

[10] R. Scheiber and A. Moreira, "Improving co-registration accuracy of interferometric SAR images using spectral diversity," in *Proc. IGARSS'99*, Hamburg, Germany, June 1999, pp. 1709–1711.

[11] A. Monti Guarnieri and C. Prati, "An interferometric quick-look processor," *IEEE Trans. Geosci. Remote Sensing*, vol. 37, pp. 861–866, Mar. 1999.

[12] R. Scheiber, A. Reigber, A. Ulbricht, K. Papathanassiou, R. Horn, S. Buckreuß, and A. Moreira, "Overview of interferometric data acquisition and processing modes of the experimental airborne SAR system of DLR," in *Proc. IGARSS'99*, Hamburg, Germany, June 1999, pp. 35–37.

[13] K. Eldhuset and P. Valand, "ScanSAR processing and simulation for ASAR using ERS-1 raw data," *Int. J. Remote Sensing*, vol. 16, no. 14, pp. 2657–2674, 1995.

[14] A. Rihaczek, *Principles of High Resolution Radar*. New York: McGraw-Hill, 1969.
[15] C. Cafforio, C. Prati, and F. Rocca, "SAR data focusing using seismic migration techniques," *IEEE Trans. Aerosp. Electron. Syst.*, vol. 27, pp. 194–207, Mar. 1991.
[16] R. Raney, H. Runge, R. Bamler, I. Cumming, and F. Wong, "Precision SAR processing using chirp scaling," *IEEE Trans. Geosci. Remote Sensing*, vol. 32, pp. 786–799, July 1994.
[17] A. Moreira, J. Mittermayer, and R. Scheiber, "Extended chirp scaling algorithm for air- and spaceborne SAR data processing in stripmap and ScanSAR imaging modes," *IEEE Trans. Geosci. Remote Sensing*, vol. GE-34, pp. 1123–1136, Sept. 1996.
[18] R. Raney, "A new and fundamental Fourier transform pair," in *Proc. IGARSS*, Clear Lake, TX, 1992, pp. 106–107.
[19] M. Sack, M. Ito, and I. Cumming, "Application of efficient linear FM matched filtering algorithms to synthetic aperture radar processing," in *Proc. Inst. Elect. Eng. F*, vol. 132, Feb. 1985, pp. 45–57.
[20] H. Zebker and J. Villasenor, "Decorrelation in interferometric radar echoes," *IEEE Trans. Geosci. Remote Sensing*, vol. GE-30, pp. 950–959, Sept. 1992.
[21] D. Just and R. Bamler, "Phase statistics of interferomgrams with applications to synthetic aperture radar," *Appl. Opt.*, vol. 33, no. 20, pp. 4361–4368, July 1994.
[22] M. Bara, R. Scheiber, A. Broquetas, and A. Moreira, "Interferometric SAR signal analysis in the presence of squint," *IEEE Trans. Geosci. Remote Sensing*, vol. 38, pp. 2164–2178, Sept. 2000.
[23] F. Gatelli, A. Monti Guarnieri, F. Parizzi, P. Pasquali, C. Prati, and F. Rocca, "The wavenumber shift in SAR interferometry," *IEEE Trans. Geosci. Remote Sensing*, vol. 32, pp. 855–865, July 1994.
[24] E. Rodriguez and J. Martin, "Theory and design of interferometric synthetic aperture radars," in *Proc. Inst. Elect. Eng. F*, vol. 139, Apr. 1992, pp. 147–159.
[25] J. Lee, K. Papathanassiou, T. Ainsworth, M. Grunes, and A. Reigber, "A new technique for noise filtering of SAR interferometric phase imgaes," *IEEE Trans. Geosci. Remote Sensing*, vol. 36, pp. 1456–1465, June 1998.
[26] B. Reeves, J. Homer, G. Stickley, D. Noon, and I. Longstaff, "Spatial vector filtering to reduce noise in interferometric phase images," in *Proc. IGARSS'99*, Hamburg, Germany, June 1999.
[27] R. Bamler, "Interferometric stereo radargrammetry: Absolute height determination from ERS-ENVISAT interferograms," in *Proc. IGARSS*, Honolulu, HI, July 2000.
[28] D. Imel, "Accuracy of the residual-delay absolute-phase algorithm," *IEEE Trans. Geosci. Remote Sensing*, vol. 36, pp. 322–324, Jan. 1998.
[29] R. Bamler, D. Geudtner, B. Schättler, P. Vachon, U. Steinbrecher, J. Holzner, J. Mittermayer, H. Breit, and A. Moreira, "Radarsat ScanSAR interferometry," in *Proc. IGARSS'99*, Hamburg, Germany, June 1999.
[30] A. Monti Guarnieri and F. Rocca, "Combination of low- and high-resolution SAR images for differential interferometry," *IEEE Trans. Geosci. Remote Sensing*, vol. 37, pp. 2035–2049, July 1999.
[31] J. Mittermayer, A. Moreira, and O. Loffeld, "Spotlight SAR data processing using the frequency scaling algorithm," *IEEE Trans. Geosci. Remote Sensing*, vol. 37, pp. 2198–2214, Sept. 1999.
[32] R. Lanari, S. Hensley, and P. Rosen, "Chirp z-transform based SPECAN approach for phase-preserving ScanSAR image generation," *Proc. Inst. Elect. Eng., Radar, Sonar Navig.*, vol. 145, pp. 254–261, Oct. 1998.
[33] R. Bamler and M. Eineder, "ScanSAR processing using standard high precision SAR algorithms," *IEEE Trans. Geosci. Remote Sensing*, vol. 34, pp. 212–218, Jan. 1996.
[34] A. Monti Guarnieri and C. Prati, "ScanSAR focusing and interferometry," *IEEE Trans. Geosci. Remote Sensing*, vol. 34, pp. 1029–1038, July 1996.
[35] R. Horn, "The DLR airborne SAR project E-SAR," in *Proc. IGARSS*, Lincoln, NE, 1996, pp. 1624–1628.
[36] K. Papathanassiou, A. Reigber, R. Scheiber, R. Horn, A. Moreira, and S. Cloude, "Airborne polarimetric SAR interferometry," in *Proc. IGARSS*, Seattle, WA, 1998.

Rolf Scheiber received the Diploma degree in electrical engineering from the Technical University of München, München, Germany, in 1994, doing his thesis on the estimation of the Doppler parameters for the 2-D SAR processing.

In 1994, he was with at the Institute for Communications Technology, German Aerospace Center (DLR), Oberpfaffenhofen, Germany, on channel measurements for mobile satellite communications. Since 1995, he has been with the Signal Processing Group, Institute for Radio Frequency Technology, DLR, as a Research Scientist. He developed an operational high precision interferometric SAR processing algorithm for airborne data and is presently responsible for the operational interferometric processing of the experimental SAR system of DLR (E-SAR).

Mr. Scheiber was awarded as a co-author with the 1996 GRSS Transactions Prize Paper Award for the contribution "Extended Chirp Scaling Algorithm for Air- and Spaceborne SAR Data Processing in Stripmap and ScanSAR Imaging Modes," in 1997. His current research interests include algorithm development for air- and spaceborne SAR interferometry, interferometric performance estimation, and algorithm development for real-time processing for future spaceborne SAR sensors.

Alberto Moreira (M'92–S'96) was born in São José dos Campos, Brazil, in 1962. He received the B.S.E.E. and the M.S.E.E. degrees in 1984 and 1986, respectively, from the Aeronautical Technological Institute (ITA), Brazil, and the Eng. Dr. degree ("mit Auszeichung"—Hons.) from the Technical University of Münich, Münich, Germany, in 1993.

In 1987, he received a four-year scholarship from DAAD, Germany, to work toward the Ph.D. at the German Aerospace Center (DLR - Institut für Hochfrequenztechnik) in the area of SAR signal processing. From 1985 to 1986, he was with ITA as a Research Assistant and Consultant. From 1992 to 1995, he was the Head of the Signal Processing Group with DLR and was responsible for the development of a high resolution real-time airborne SAR processor. As Chief Scientist and Engineer with DLR since 1996, he manages the DLR SAR Technology Department. Under his leadership, the DLR airborne SAR system has been upgraded to operate in innovative imaging modes like polarimetric SAR interferometry and polarimetric SAR tomography. He is currently serving as a member of the Administrative Committe of the Geoscience and Remote Sensing Society.

Dr. Moreira was the recipient of the DLR Science Award in 1995. In 1996, he and his colleagues received the IEEE 1996 Transactions Prize Paper Award for the development of the so-called "Extended Chirp Scaling Algorithm." In 1999, he received the IEEE AESS Fred Nathanson Memorial Award to the Young Radar Engineer of the Year. His professional interests and research areas encompass SAR end-to-end system design and analysis, SAR signal processing and interferometry, innovative radar techniques, and expert systems for data fusion and classification.